PROTEINS
STRUCTURE ■ FUNCTION ■ BIOINFORMATICS

Crystal structure of Natratoxin, a novel snake secreted phospholipaseA2 neurotoxin from *Naja atra* venom inhibiting A-type K^+ currents

Pu Hu,[1] Lei Sun,[2,3] Zhi-Qiang Zhu,[2,3] Xiao-Wei Hou,[2,3] Shu Wang,[1] Shan-Shan Yu,[1] Hui-Li Wang,[1] Ping Zhang,[2,3] Ming Wang,[1] Li-Wen Niu,[2,3] Mai-Kun Teng,[2,3]* and Di-Yun Ruan[1]*

[1] Department of Neurobiology and Biophysics, School of Life Sciences, University of Science and Technology of China, HeFei, Anhui, 230027, People's Republic of China

[2] Hefei National Laboratory for Physical Sciences at Microscale, HeFei, Anhui, People's Republic of China

[3] Department of Molecular and Cell Biology, School of Life Sciences, University of Science and Technology of China, HeFei, Anhui, 230027, People's Republic of China

ABSTRACT

Snake secreted phospholipasesA2 (sPLA2s) are widely used as pharmacological tools to investigate their role in diverse pathophysiological processes. Some members of snake venom sPLA2s have been found to block voltage-activated K^+ channels (K_v channels). However, most studies involved in their effects on ion channels were indirectly performed on motor nerve terminals while few studies were directly done on native neurons. Here, a novel snake sPLA2 peptide neurotoxin, Natratoxin, composed of 119 amino acid residues and purified from Naja atra venom was reported. It was characterized using whole-cell patch-clamp in acutely dissociated rat dorsal root ganglion (DRG) neurons. It was found to effectively inhibit A-type K^+ currents and cause alterations of channel gating characters, such as the shifts of steady-state activation and inactivation curves to hyperpolarization direction and changes of $V_{1/2}$ and slope factor. Therefore, Natratoxin was suggested to be a gating modifier of K_v channel. In addition, this inhibitory effect was found to be independent of its enzymatic activity. These results suggested that the toxin enacted its inhibitory effect by binding to K_v channel. To further elucidate the structural basis for this electrophysiological phenomenon, we determined the crystal structure of Natratoxin at 2.2 Å resolution by molecular replacement method and refined to an R-factor of 0.190. The observed overall fold has a different structural organization from other K^+ channel inhibitors in animal toxins. Compared with other K_v channel inhibitors, a similar putative functional surface in its C-terminal was revealed to contribute to protein–protein interaction in such a blocking effect. Our results demonstrated that the spatial distribution of key amino acid residues matters most in the recognition of this toxin towards its channel target rather than its type of fold.

Proteins 2008; 72:673–683.

***Key words:** snake venom sPLA2s; A-type K^+ currents; dorsal root ganglia; whole-cell patch clamp; X-ray structure; conformation.*

INTRODUCTION

Voltage-activated K^+ channels (K_v channels) are present in almost all phylogenetic classes and widely distributed in many cell types[1,2] where they are involved in fundamental physiological processes. They are tetrameric membrane proteins that open and close a K^+ selective pore in response to changes in membrane voltage,[3,4] and produce a rapid activation and rapid inactivation of K^+

The Supplementary Material referred to in this article can be found online at http://www.interscience.wiley.com/jpages/0887-3585/suppmat/

Abbreviations: DRG, dorsal root ganglion; I_A, A-type K^+ currents; K_v channel, voltage activated K^+ channel; sPLA2, secreted phospholipaseA2.

Grant sponsor: The National Nature Science Foundation of China; Grant numbers: 30630057, 30121001, 30670554, 30670662, 30300288, 30025012; Grant sponsor: The National Basic Research Program of China; Grant number: 2002CB512907; Grant sponsor: Academia Sinica; Grant number: KZCX3-SW-437; Grant sponsor: Anhui Provincial National Science Foundation; Grant number: 050430801

Pu Hu and Lei Sun contributed equally to this work.

*Correspondence to: Mai-Kun Teng or Di-Yun Ruan, School of Life Sciences, University of Science and Technology of China, Hefei, Anhui 230027, People's Republic of China. E-mail: mkteng@ustc.edu.cn or ruandy@ustc.edu.cn

Received 19 August 2007; Revised 5 December 2007; Accepted 6 December 2007
Published online 4 February 2008 in Wiley InterScience (www.interscience.wiley.com). DOI: 10.1002/prot.21964

currents upon depolarization of cell membrane. The secondary structure of each of the four repeating monomers forming K_v channels has six α-helix segments, which are divided into a voltage-sensing domain (S1–S4) and an ion-conducting pore domain (S5–S6).[5–8] Animal peptide toxins acting on K_v channels have provided extensive use concerning the physiology of K_v channels. They are mostly present in limited amounts in venoms of various species, such as snakes,[9] sea anemones, spiders,[10] scorpions,[11] honey bees,[12] and snails of the genus Conus.[13] Detailing the structures and functions of various animal toxins has provided us with a lot of uses in terms of protein engineering and therapeutic potential.[14–16] Because toxins often display a large array of ion channel targets, of which only one may be of therapeutic value, a detailed examination of their folds and molecular determinants offers potential to alter their pharmacological selectivity, specificity and potency.[17]

Recently, we have identified a novel snake peptide toxin, Natratoxin, purified from *Naja atra* venom, as a member of snake secreted phospholipasesA2 (sPLA2s) family. Secreted phospholipasesA2 (EC 3.1.1.4) comprise a family of structurally conserved enzymes catalyzing hydrolysis of glycerophospholipids from membrane phospholipids at *sn*-2 position to release free fatty acids and lysophospholipids.[18] Most sPLA2s share a common set of structural features including a small molecular mass (14–19 kDa), a compact structure with several disulfides, and a conserved Ca^{2+}-dependent catalytic mechanism.[19] They were found in insect, snake venoms, mammalian tissues, plants, bacteria, fungi, and viruses.[18,20–24] Among them, snake venom sPLA2s are widely used as pharmacological tools to investigate their role in diverse pathophysiological processes. Many of them display a wide spectrum of toxic effects including neurotoxic, myotoxic, cardiotoxic, cytotoxic, anticoagulant, convulsant, hypotensive, and proinflammatory effects.[23,25–28] Previous electrophysiological investigations have suggested that PLA2 neurotoxins from snake venoms can increase the release of acetylcholine (Ach) at the neuromuscular junction by blocking voltage-gated K^+ channels (K_v channels) in motor nerve terminals.[29–31] However, there have been few direct demonstrations of their K^+ channel blocking actions and most reports are only about the effects of β-bungarotoxin (β-BuTX). Most studies involved in their effects on ion channels were indirectly performed on motor nerve terminals while few studies were directly done on native neurons, except β-bungarotoxin (β-BuTX) and β-agkistrodotoxin (β-AgTx). The former was shown to block non-inactivating voltage-dependent K^+ currents in dorsal root ganglion neurons of the guinea pig,[29] and the latter has been reported to inhibit large-conductance calcium-activated K^+ channels in rat hippocampal CA1 pyramidal neurons.[32] Hence, it is reasonable to wonder whether this newly purified snake venom sPLA2 has any effect on K^+ channel in neurons. Interestingly, our recent experiments showed that Natratoxin has an effectively inhibitory effect on A-type K^+ currents in acutely dissociated rat dorsal root ganglion (DRG) neurons. In addition, this inhibitory effect was found to be independent of its enzymatic activity. To clarify the structural basis for the electrophysiological function, we further determined its three dimensional crystal structure. In this article, we will report the electrophysiological function and 3D solution crystal structure of Natratoxin.

MATERIALS AND METHODS

Protein purification

Tissues from *Naja atra* venom gland were obtained from the southern mountain region, Anhui, China. Natratoxin was purified from *Naja atra* venom on CM and DEAE Sephacel ion-exchange columns at 8°C. The venom was dissolved in 20 m*M* Tris-HCl, pH 8.0, and centrifuged at 12,000 rpm/min for 20 min to remove insoluble portion. The supernatant was collected and diluted with the same buffer. The diluted sample was loaded onto a CM Sephacel cation-exchange column. The column was washed with 20 m*M* Tris-HCl, pH 8.0, to remove unbound fractions at a rate of 1 mL/min. The gradient was run from 0 to 0.5 *M* NaCl in 20 m*M* Tris-HCl, pH 8.0. The elution profile showed 10 major peaks. The second peak were dialyzed against 70 m*M* Tris-HCl buffer pH 8.0 (A solution) and then loaded onto a diethylaminoethyl (DEAE) Sephacel anion-exchange column. To elute Natratoxin, a salt gradient of 0.0–1.0 *M* NaCl (B solution) was used. Fractions with PLA2 activity were eluted at 14.3% B solution and dialyzed against deionized water to remove salt. The purity of the protein was identified by mass spectrometry and SDS-PAGE.

Complete protein sequence determination

The venom gland was homogenized in Rizol (Bio Basic) in ice-cold conditions. The total RNA was extracted using the SV total RNA isolation kit (Promega). AMV single step RT-PCR kit was used for the PCR amplification of the gene. The sequence of Natratoxin's N-terminus was determined by the Edman degradation method as implemented on an Applied Biosystems Procise 491 protein sequencer, and was used for the design of primers. From the primers we got the cDNA sequence by 3′-Full race core set (TaKaRa) to reduce the protein amino acid sequence. The PCR was carried out in accordance with the manufacturer's instructions and the single PCR products were isolated from agarose gels using Concert rapid gel extraction system (Invitrogen, USA), then cloned into the pGEM-T EASY vector (Promega, USA) and sequenced.

Crystallization and data collection

Diamond-shaped crystals were obtained at 281 K by vapor diffusion in 1–4 μL hanging drops for one week. Each drop contained equal volumes of protein solution (12 mg/mL) and reservoir solution containing 2.0 *M* ammonium sulfate, 5% v/v iso-propanol. The X-ray intensity data were collected by a MAR Research 345-mm imaging-plate scanner mounted on a MAR X160 rotating-anode X-ray generator (Marresearch, Germany). The data was integrated by MOSFLM[33] and further processed with programs from the CCP4 package.[34] A complete data set to 2.2 Å resolution was obtained using a single crystal. The full data set has an R_{sym} of 5.2% and completeness of 97%. All the data were measured from the frozen crystal cryoprotected in 80% reservoir solution and 20% glycerin. Crystals are formed in space group $P4_1$, with unit-cell dimensions of $a = 42.078$ Å, $b = 42.078$ Å, $c = 64.117$ Å, and one molecule per asymmetric unit.

Model building and refinement of crystallization structure

The crystal structure of Natratoxin was determined by the molecular replacement method with Molrep from the CCP4 software suite using the model of nPLA2 (PDB code: 1PSH[35]). The top peak in both the rotation and translation functions gave the best solution in the correct space group $P4_1$. At the beginning of the refinement, residues with unclear side chain electron density were mutated to alanines and water molecules were not included in the model. The refinement was carried out with Refmac from the CCP4 software suite. In each step, the model was examined and corrected manually by inspection of $2F_o–F_c$ and $F_o–Fc$ electron density maps using the graphics Program O.[36] When the *R*-factor reached 23.4%, water molecules were gradually identified and inserted into the model according to the electron density map. The water molecules were adjusted manually for good hydrogen bonding geometry and interactions with protein atoms. The overall assessment of model quality was performed using PROCHECK,[37] and the atomic coordinates have been deposited in the Protein Data Bank as entry 2OSH.

Enzymatic activity determination

To determine the enzymatic activity of Natratoxin, we used phenol red as indicator to measure the carboxyl produced by hydrolyzing lecithin. The composition of standard solution was as follows: 0.055 m*M* phenol red, 100 m*M* NaCl, 7 m*M* Triton X-100, 0.175% lecithin, 5 m*M* Tris-HCl, pH 7.9. Every 10 μg Natratoxin was added to 3 mL standard solution, then scan at 558 nm with DU 640 Nucleic Acid and Protein Analyzer. In Ca^{2+} solution, 10 m*M* $CaCl_2$ was added into the standard solution; in EDTA solution 5 m*M* EDTA was added.

Cell preparation for electrophysiological technique

DRG from 15–21 days' Wistar rats were dissected and incubated in the fresh Dulbecco's modified Eagle's medium (DMEM, Gibco) solution, which was added with 1 mg/mL type II collagenase (Sigma) for 1 h at 32 ± 1°C. The collagenase was then removed and the ganglia were washed three times with the DMEM solution. Further incubation for 50 min at 32 ± 1°C was performed by supplementing 0.5 mg/mL type IX trypsin (Sigma), to the incubation solution. The trypsin was removed and the ganglia were washed three times with the standard external solution (see below). The ganglia were transferred to 1.0 mL standard external solution with DNase (Sigma, type I, 0.1 mg/mL external solution) added. The ganglia were dissociated by trituration with a series of fire-polished Pasteur pipettes. DRG neurons were placed in several dishes. Thirty minutes later, when the neurons were attached to the bottom, they were used for recordings at room temperature (20–25°C).

The rats were obtained from the Laboratory Animal Center, University of Science and Technology of China, Hefei, China. All experiments were conducted in accordance with the National Institutes of Health Guide for the Care and Use of Laboratory Animals. All efforts were made to minimize the number of animals used and their suffering.

Solutions and drugs

The composition of standard external solution was as follows: 140 m*M* NaCl, 4 m*M* KCl, 2 m*M* $CaCl_2$, 1 m*M* $MgCl_2$, 10 m*M* HEPES, and 10 m*M* D-glucose. Recording external solution: 90 m*M* choline chloride, 50 m*M* tetraethylammonium chloride (TEA), 4 m*M* KCl, 2 m*M* $CaCl_2$, 1 m*M* $MgCl_2$, 0.2 m*M* $CdCl_2$, 10 m*M* HEPES, and 10 m*M* D-glucose, 0.5 m*M* tetrodotoxin (TTX). The pH of each external solution was adjusted to 7.3–7.4 with Tris-base and the osmolarity was adjusted to 305–310 mmol/kg using sucrose. Both external solutions were preoxygenated before use. The high concentration of TEA was included to reduce delayed rectifier sustained currents, thus facilitate observation of A-type K^+ components. Voltage-gated calcium currents were blocked by application of 0.2 m*M* $CdCl_2$. Pipette solution for whole-cell recording: 140 m*M* KCl, 4 m*M* NaCl, 1 m*M* $MgCl_2$, 10 m*M* EGTA, 10 m*M* HEPES, and 2 m*M* Na_2-ATP. The osmolarity was adjusted to 300–305 mmol/kg with sucrose, and the pH was adjusted to 7.2 with Tris-base.

Toxin stock solutions were prepared in deionized water. They were stored frozen at −20°C in small ali-

quots for no more than 1 week and were diluted to each desired concentration with recording external solution just before experiment. Drugs were applied via a Y-tube microperfusion system. By applying this method, the external solution surrounding a neuron could thus be completely exchanged within 20 ms. The tip of the superfusion pipette was normally placed 50–100 μm away from the cell, a position that allowed rapid as well as uniform drug application and preserved the mechanical stability of the cell.

Patch clamp recordings

The electrophysiological recordings were performed with the conventional whole-cell voltage-clamp recording configuration. Patch pipettes were pulled from glass capillaries with an outer diameter of 1.5 mm on a two-stage puller (PP-830, Narishige, Tokyo, Japan), and had resistance of 2–5 MΩ when filled with pipette solution. Data were acquired with a PC-IIC patch-clamp amplifier (HUST-IBB, Wuhan, China) connected to a computer via an ITC-16 computer interface (Instrutech, NY), digitized at 20 kHz, filtered at 2 kHz, stored in a computer hard disk. Cells were considered only when the seal resistance was more than 1 GΩ and the series resistance (less than 30 MΩ) changed less than 20% throughout the experiment. Fast and slow capacitances were neutralized and series resistance was always compensated for over 85% with internal voltage-clamp circuitry.

Data analysis

Data analysis was executed using pClampfit 8.0 and Origin 7.5 software programs.

The voltage dependence of activation was determined using standard protocols. The conductance $G\ (V)$ was calculated according to: $G\ (V) = I(V)/(V - V_k)$ where V_k is the K^+ reversal potential, V the command potential, and $I\ (V)$ the peak current amplitude. $G\ (V)$ was then fitted with the following Boltzmann equation: $G/G_{max} = 1/\{1 + \exp[(V_{1/2} - V)/K_m]\}$ where G_{max} is the maximum K^+ conductance, $V_{1/2}$ is the voltage where G is the half of G_{max}, and K_m indicates the slope of the relationship between channel activation and membrane voltage.

Steady-state inactivation curves were obtained with a Boltzmann fit of the data using $I/I_{max} = 1/\{1 + \exp[(V_{1/2} - V)/K_m]\}$ where I/I_{max} is the normalized current, $V_{1/2}$ is the voltage potential for half-maximal inactivation, and K_m indicates the slope factor.

All the experimental values were presented as mean ± S.E.M. Statistical analysis was performed using the Student's *t*-test with paired comparisons, and P values less than 0.05 were considered significant. The each n represents the number of neurons examined.

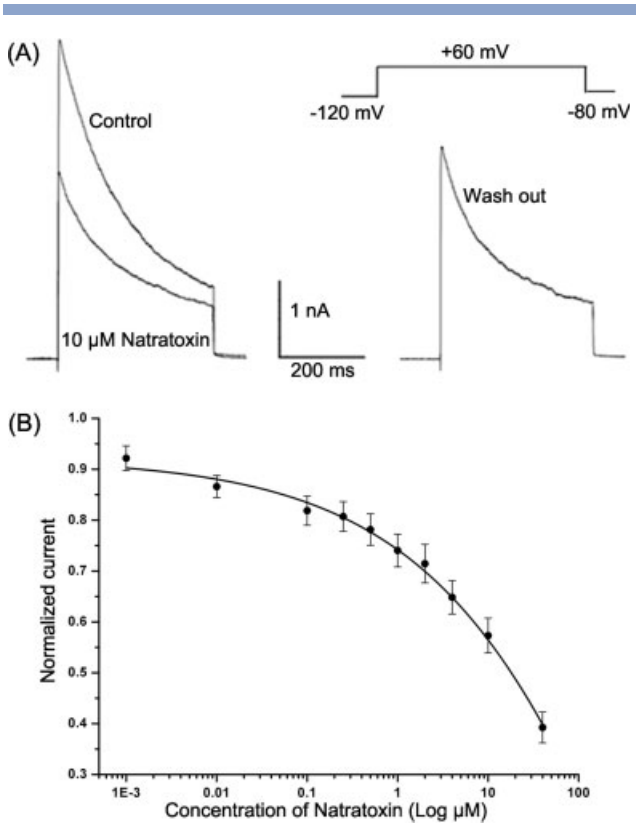

Figure 1

*Natratoxin decreased I_A currents in a concentration-dependent manner. (**A**) Representative traces before and after external application of 10 μM Natratoxin in the same neuron. I_A currents were partially recovered after washout. (**B**) Concentration–response curve for different doses of Natratoxin at +60 mV. Concentrations were plotted as on a semilogarithmic scale. Each point represents the mean ± S.E.M. of seven to eight measurements.*

RESULTS

Natratoxin inhibited A-type K^+ currents in DRG neurons in a concentration-dependent manner

I_A was recorded in medium-sized DRG neurons (35–40 mm diameter) in the presence of 50 m*M* TEA to block delayed rectifier potassium currents (I_k). At a holding potential of −80 mV, currents were elicited by stepping membrane potential to +60 mV for 400 ms from a 500 ms preconditioning pulse potential of −120 mV at least 5 min after the patched membrane was ruptured. Natratoxin was diluted in recording solution to each desired concentration just before experiment. Various concentrations of Natratoxin were applied extracellularly only I_A currents were stable. As illustrated in Figure 1(A), the average current amplitude was reduced to 57 ± 3% (n = 8, $P < 0.05$) with 10 μ*M* Natratoxin compared with controls, and recovered to 66 ± 3% (n = 8, $P < 0.05$) of control after washout with control external solution.

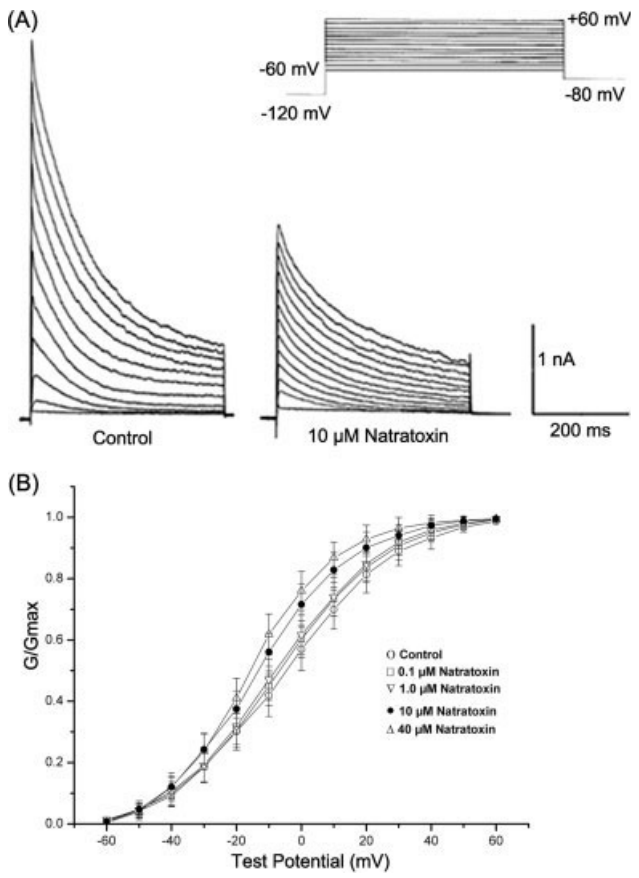

Figure 2

*Effect of Natratoxin on the activation curve of I_A. (**A**) Current traces were shown in the same neuron before and after 10 μM Natratoxin. (**B**) The ratio of normalized conductance (G/G_{max}) was plotted against various test potentials. Data points were fitted with Boltzmann equations. Data are expressed as mean ± S.E.M. ($n = 7$).*

As illustrated in Figure 1(B), various concentrations of Natratoxin decreased I_A amplitude with increasing doses, indicating the inhibitory effects were dose-dependent. Currents could be partially recovered.

Voltage-dependent activation of A-type K^+ currents

Voltage commands from −60 mV to +60 mV in increments of 10 mV following a −120 mV prepulse were used. A representative response under control and after exposure to 10 μ*M* Natratoxin was shown in Figure 2(A). The responses of different neurons tested in control or in the presence of Natratoxin were normalized with respect to the corresponding maximum currents obtained at +60 mV and depicted in Figure 2(B). I_A was plotted as a function of test depolarizing voltage steps. Each of the normalized curves was fitted with a single Boltzmann equation. The values of $V_{1/2}$ and slope factor k were described in Table I. The hyperpolarizing shifts of parameters increased with increasing concentrations.

Steady-state inactivation of A-type K^+ currents

The effect of 10 μ*M* Natratoxin on the steady-state inactivation was shown in Figure 3(A) examined with a double-pulse protocol. An 80-ms prepulse (−120 to −10 mV) from the holding potential of −80 mV was followed by a 400 ms test depolarization of +60 mV. The current amplitude normalized to the maximum current in each concentration group was calculated as I/I_{max}, and plotted versus prepulse voltage [depicted in Figure 3(B)]. Curves were fitted by a single Boltzmann equation. The values of $V_{1/2}$ and slope factor k were presented in Table I. The hyperpolarizing shifts of parameters increased with increasing concentrations.

The inhibitory effect was independent of the enzymatic acitivity

Through the hydrolytic action, sPLA2 causes arachidonic acid (AA) to be liberated from phospholipids. AA has been shown to suppress I_A in rat CA1 hippocampal pyramidal cells.[38,39] Since Ca^{2+} is essential for the enzymatic activity of all the sPLA2s, including Natratoxin (data was shown in the supporting information), to explore whether the inhibitory effect of Natratoxin on I_A was dependent on the enzymatic activity, we investigated

Table I

The Effect of Natratoxin on the Activation and Inactivation Parameters of Voltage-Gated A-Type Potassium Currents (I_A)

	Activation ($n = 7$)		Inactivation ($n = 7$)	
	$V_{1/2}$ (mV)	K (mV)	$V_{1/2}$ (mV)	K (mV)
Control	−5.0 ± 2.8	18.3 ± 2.8	−80.5 ± 0.9	9.3 ± 0.9
0.1 μ*M* Natratoxin	−6.6 ± 2.3	17.0 ± 2.2	−83.5 ± 2.5	9.4 ± 0.6
1.0 μ*M* Natratoxin	−7.4 ± 2.4	16.7 ± 2.2	−88.4 ± 1.4[a]	10.7 ± 1.2
10 μ*M* Natratoxin	−13.5 ± 2.2[a]	15.4 ± 2.0[a]	−93.0 ± 2.6[b]	11.6 ± 1.8[a]
40 μ*M* Natratoxin	−15.4 ± 2.1[b]	13.5 ± 1.7[a]	−97.7 ± 3.7[b]	13.1 ± 1.6[a]

$V_{1/2}$, voltage at half-maximal activation or inactivation; K, slope factor.
[a]Significantly, $P < 0.05$ versus control.
[b]Significantly, $P < 0.01$ versus control.

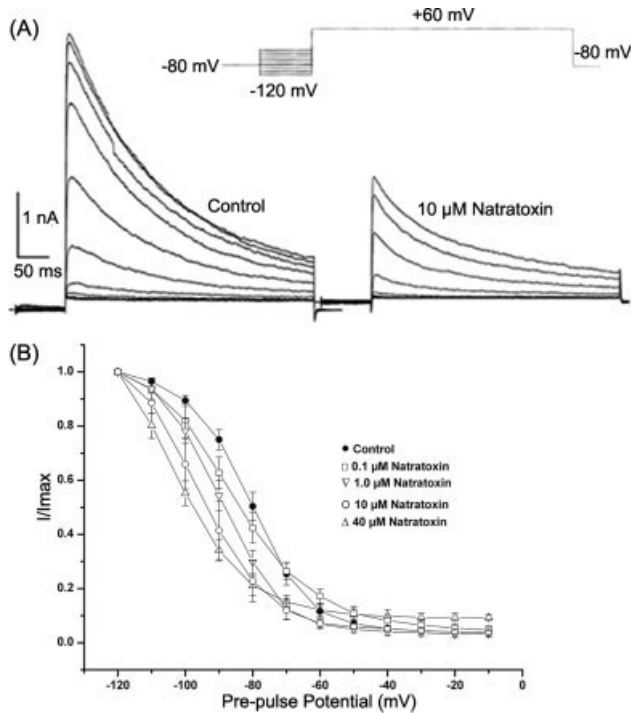

Figure 3

*Effect of Natratoxin on the steady-state inactivation of I_A. (**A**) Current traces shown were recorded in the same neuron before and after external application of 10 μM Natratoxin. (**B**) Normalized I/I_{max} was plotted against the prepulse voltage. Data points were fitted with Boltzmann equations. Data are expressed as mean ± S.E.M. ($n = 7$).*

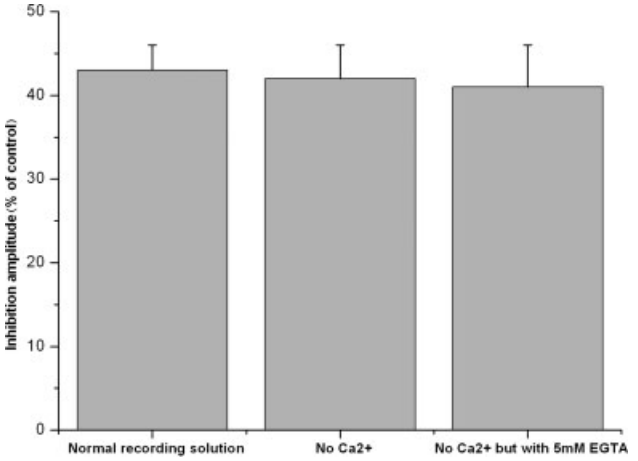

Figure 4

The inhibitory effect of Natratoxin on I_A was independent of the enzymatic activity. To rule out enzymatic effects, Natratoxin was diluted in one recording solution without Ca^{2+} ($n = 8$) and another solution also without Ca^{2+} but with 5 mM EGTA added in ($n = 8$). In both cases, inhibitory effects were not significantly different from those observed in control tests ($n = 8$, both $P > 0.05$).

the action of Natratoxin without Ca^{2+}. Natratoxin was diluted in one recording solution without Ca^{2+} and another solution also without Ca^{2+} but with 5 m*M* EGTA added in. Cells were incubated in standard solution without Ca^{2+} for at least 5 min before test. As illustrated in Figure 4, 10 μ*M* Natratoxin decreased I_A by 42 ± 4% ($n = 8$, $P > 0.05$) and 41 ± 5% ($n = 8$, $P > 0.05$) in each case, respectively, not significantly different from 43 ± 3% ($n = 8$) observed in control tests. Therefore, the possibility of AA's effect was excluded.

Quality of the model

The final model consists of 973 atoms and 65 water molecules that exhibits a crystallographic *R*-factor of 19.0% and a *R*-factor of 24.2% for all data in the resolution range of 20.0–2.2 Å. The stereochemical quality of the model as defined by program PROCHECK[37] indicates that 89.3% of residues fall in the most favored regions of the Ramachandran plot. The remaining 10.7% residues were found in the additionally allowed regions. The average B value for all the atoms was 19.3 $Å^2$, and atomic coordinates have been deposited in the Protein Data Bank as entry 2OSH. Data collection statistics and refinement statistics were described in Table II.

Table II

Data Collection and Model Refinement Statistics

Data collection	
Space group	$P4_1$
Unit cell dimensions (Å) and angles (°)	$a, b, c = 42.08, 42.08, 64.12$ $\alpha = \beta = \gamma = 90$
Solvent content (%)	42.01
Total number of measured reflections	11,105
Resolution range (Å)	20–2.20
The highest resolution shell (Å)	2.32–2.20
R_{sym} (%)[a]	5.2 (12.7)
I/σ	13 (8.0)
Completeness (%)[b]	97.4 (98.7)
Refinement	
Number of unique reflections	5555
Number of reflections for Rfree	264
R_{cryst} (%)[c]	19.0
R_{free} (%)[d]	24.2
Nonhydrogen protein atoms	908
Water molecules	65
R_{msd} from ideal values for bond length (Å)	0.012
R_{msd} from ideal values for bond angle(°)	1.224
Average isotropic B factors($Å^2$)	19.30
Ramachandran statistics	
Fully allowed regions (%)	89.3
Addition allowed regions (%)	10.7

Values in parentheses are for the highest resolution shell.

[a] $R_{sym} = \Sigma h \Sigma j \, |<I(h)> - I(h)j| / \Sigma h \Sigma j \, I(h)j$, where $I(h)j$ is the jth observed reflection intensity and $<I(h)>$ is the mean intensity of reflection h.

[b] The completeness is the ratio of number of observed reflections to that of possible reflections.

[c] $R_{cryst} = \sum ||F_{obs}| - |F_{calc}|| / \sum |F_{obs}|$, where F_{obs} and F_{calc} are observed and calculated structure factors.

[d] $R_{free} = \sum_T ||F_{obs}| - |F_{calc}|| / \sum_T |F_{obs}|$, where T is a test data set of about 10% of the total reflections randomly chosen and set aside prior to refinement.

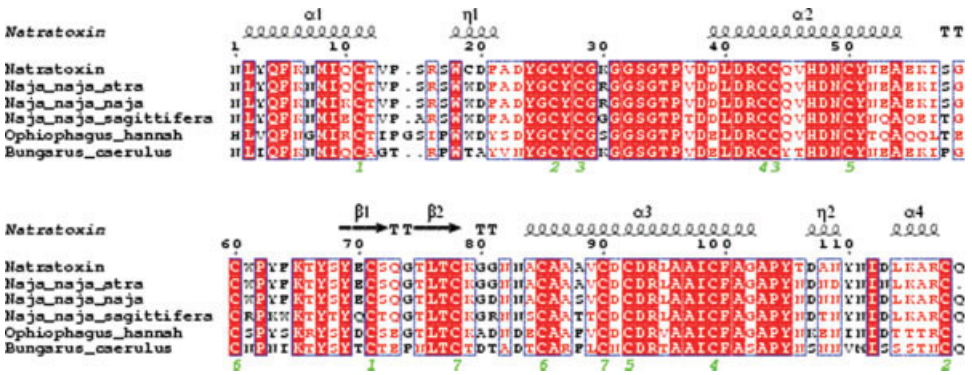

Figure 5

Sequence comparison of Natratoxin with other PLA2s. The identical residues are shown in reversed character. Digits under each column indicate seven disulfide bridges: (1) Cys11-Cys71, (2) Cys26-Cys118, (3) Cys28-Cys44, (4) Cys43-Cys109, (5) Cys50-Cys92, (6) Cys60-Cys85, and (7) Cys78-Cys90. [Color figure can be viewed in the online issue, which is available at www.interscience.wiley.com.]

Overall Natratoxin structure

The molecular topology of Natratoxin conserves all the main features of PLA2-type (see Fig. 5). As was shown in Figure 6(A), the overall structure of Natratoxin contains six helices and a double-stranded antiparallel β-sheet, which is stabilized by seven disulfide bridges. The six helices are composed of an N-terminal helix 1 (H1) from residues 2 to 12, helix 2 (H2) from residues 39 to 55 and helix 3 (H3) from residues 84 to 102 and three helical short turns involving residues 19–21 (SH4), 107–109 (SH5), and 114–116 (SH6) that is an abnormal helical short turns in PLA2s [Figure 6(A)]. The double-stranded antiparallel β-sheet is observed for residues 69–72 and 75–78. The sequence comparisons of Natratoxin with PLA2s from other Naja subspecies such as *Naja naja naja* (nPLA2), *Naja naja atra* (aPLA2), *Naja naja kouthia* (kPLA2), *Naja naja sputatrix* (tPLA2), *Naja melanoleuca melanoleuca* (mPLA2), *Naja mossambica mossambica* (zPLA2), and *Naja naja nigricollis* (gPLA2) show sequence identities ranging from 72% to 91%. Superposition (Cα trace) with other PLA2 structures from *N. naja* subclasses such as *N. naja atra* (PDB code 1poa),[40] *N. naja kaouthia* (PDB code 1A3F),[41] and *N. naja* (PDB code 1psh)[35] shows the r.m.s. deviations of 0.67, 0.69, and 0.71 Å, respectively. These r.m.s. deviations indicate a structural conservation in the PLA2 family.

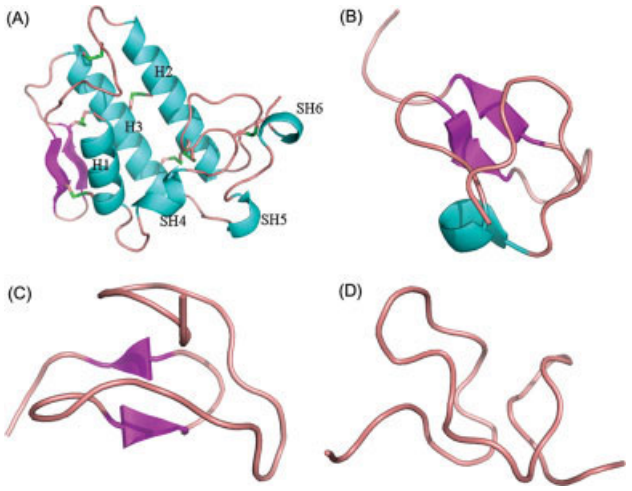

Figure 6

*Comparison of the overall fold of (**A**) Natratoxin with those of other K^+ channel inhibitors: (**B**) hatx1 (Hanatoxin1) from Grammostola spatulata, (**C**) patx1 (Phrixotoxins1) from Phrixotrichus auratus and (D) HpTX2 (Heteropodatoxin2) from Heteropoda venatoria. In (A), the model (PDB entry 2OSH) is indicated; three main helices are indicated as H1, H2 and H3, while three short helices are designated as SH4, SH5 and SH6. β-wing and disulphide linkages are also shown.*

DISCUSSION

Here, we report the electrophysiological function and crystal structure of Natratoxin, a novel snake sPLA2 peptide neurotoxin inhibiting A-type K^+ currents (I_A). The results demonstrated that Natratoxin inhibited I_A in dissociated rat DRG neurons in a concentration-dependent manner. It also caused alterations of channel gating kinetics, such as shifts of steady-state activation and inactivation curves to the hyperpolarization direction and changes of $V_{1/2}$ and slope factor. As in other neurons, I_A in DRG neurons is thought to modulate timing of repetitive action potential generation, the repolarization of single action potential, and the time required to reach threshold to fire an action potential.[42–45] In addition, I_A in DRG neurons is suggested to play an important role in nociception.[46,47] Therefore, this study may contribute to the peripheral neurotoxicity of this snake venom sPLA2 neurotoxin, such as nociceptive effects observed in

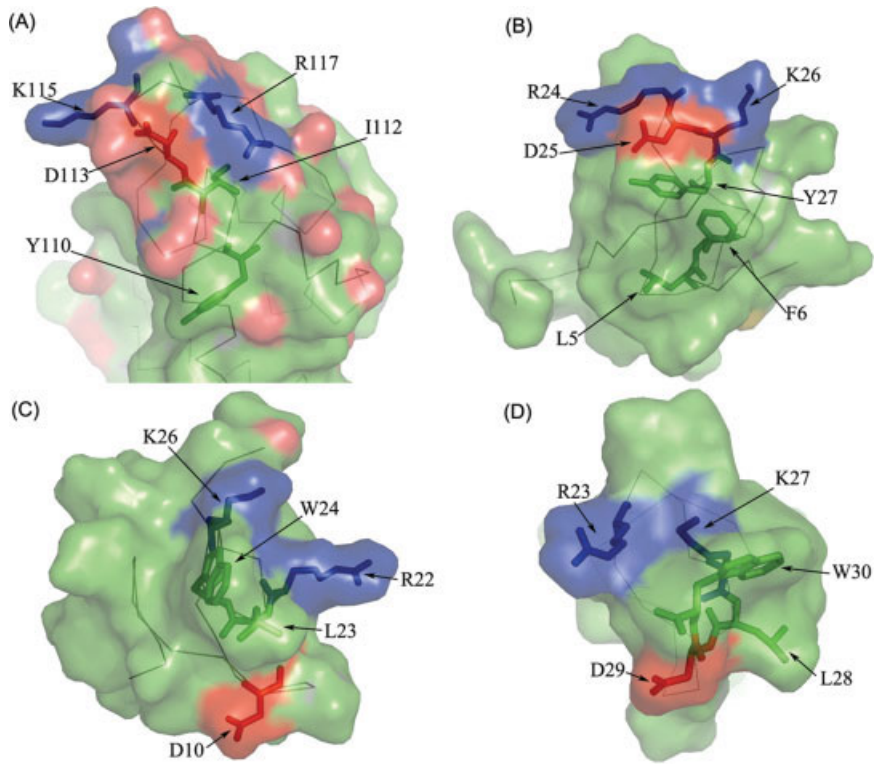

Figure 7

*Comparison of the functional surface of (**A**) Natratoxin with K^+ channel inhibitors: (**B**) Hatx1, (**C**) Patx1, and (D) HpTX2. The putative functional residues are labeled. Residues are colored as follow: blue for Lys and Arg, red for Asp and green for Leu/Ile and aromatic residues.*

human snakebite envenomations. The pharmacology of I_A in rat DRG neurons are similar to those of K_v4 (*Shal*) family of K^+ channels,[48,49] which activate at subthreshold membrane potentials, inactivate rapidly, and rapidly recover from inactivation.[39,50] Blockers of K_v channel from animal toxins have been classified into two groups: those occlude the conduction pore (pore blockers) and those modify channel gating properties (gating modifiers).[51] Here, Natratoxin not only inhibited the current amplitude of I_A but also altered channel gating kinetics, so it was suggested to be a gating modifier.

It is now clear that K_v channel can be targeted by toxins possessing unrelated folds. It has been reported that animal peptide toxins acting as K^+ channel inhibitors have different structural organizations including Csαβ (cystine stabilized alpha/beta motif) in scorpion toxins, ICK (Inhibitor Cystine Knot) in spider toxins and a short α-helix without β-sheet in bee toxins.[52,53] The ability of structurally divergent toxins to recognize a particular ion channel relies on the equivalent spatial distributions of amino acids that are key to the toxin-channel interaction.[17] Previous studies reveal that two protruding basic residues (a lysine and an arginine) serving as crucial residues'an asparagine, a methionine/isoleucine and an aromatic residue acting as influential residues are found in functional sites of all K^+ channel inhibitors, and this putative functional surface can be considered as the signature motif.[52,53] To detail the molecular basis of the intimate interaction between Natratoxin and I_A channel, we compared its structure with other K_v channel inhibitors. Compared with other K_v channel inhibitors, though the overall fold is different (as was shown in Figure 6), a very similar putative functional surface was found at its C-terminal. Figure 7 describes the putative functional surface of Natratoxin compared with other K_v channel inhibitors acting as gating modifier. In Natratoxin, Arg^{115} and Lys^{117} are the critical residues, just as Arg^{26} and Lys^{24} for hatx1, Arg^{27} and Lys^{23} for hptx2, Arg^{26} and Lys^{22} for patx1. The positively charged arginines and lysines have similar Cα distances in the four 3D structures, which are 6.10 Å for Natratoxin, 5.56 Å for hatx1, 7.10 Å for patx1, and 7.50 Å for hptx2. So, we suppose that it is not sequence distance but spatial distance between these two amino acids that helps to explain how the electrostatic interactions between positively charged residues on Natratoxin and negatively charged residues on K_v4 channel orient Natratoxin in a proper binding orientation. As shown in Figure 7, below these two positively charged

residues Arg^{115} and Lys^{117} there is an Asp^{113}, which helps Arg^{115} and Lys^{117} to form the dipole moment as a negatively charged residue. Around Asp^{113}, residues Ile^{112} and Tyr^{110} provide the possibility of local hydrophobic interactions that take place between toxin and channel and orient Natratoxin in an appropriate position.[54] So the overall physiochemical characteristics of our proposed functional surface are in good accordance with other K_v channel inhibitors. Therefore, our results supported the idea that when considering the interaction of a toxin with its ion channel target, what matters most is the spatial distribution of these key amino acid residues of the toxin, rather than its type of fold.[17]

In this study, although Natratoxin was a negatively charged peptide, the global negative charge does not affect the supposed electrostatic interaction of its positively charged residues and the negatively charged residues of the channel. Goldstein *et al.* documented this phenomenon showing that electrostatic potentials fall off quickly near protein surface, resulting in smaller effects of the global charge compared with effect of the close contact residues.[55] In addition, previous studies have also revealed that the toxic effects of venom PLA2s cannot be easily correlated with their catalytic activity, and that many venom PLA2s can exert pharmacological effects independently of their enzymatic activities.[56–59] The absence of direct correlation between catalytic activity and pharmacological effects has led to the hypothesis that the specific actions of sPLA2 are due to the presence of pharmacological sites on the sPLA2 surface which are separated from or overlap with the catalytic site.[60,61] In line with these studies, the inhibitory effect of Natratoxin on I_A was also independent of the enzymatic activity. This fact can also be explained by the presence of separated binding sites on its surface from the catalytic sites.

K_v channels produce a rapid activation and rapid inactivation of K^+ currents upon depolarization of cell membrane. Precisely defined regions have been suggested to mediate these functions. Gating modifiers of K_v channels bind to four extracellular sites near the S3 and S4 segments, close to the voltage sensor.[51] Therefore, the functional surface on the C-terminus of Natratoxin is suggested to interact with areas of I_A channel spatially close to the S4 "voltage sensor," and influence channel gating process. Binding to the resting K_v4 channel may lead to a conformationally abnormal change of channel, affect K^+ to pass through and enhance the sensitivity of voltage sensor to the depolarization of membrane potential. Therefore, peak amplitude of I_A was decreased and activation curves were shifted negatively. In addition, we also noticed a larger voltage shift of the channel inactivation than that of activation. Because the activation and inactivation processes of K_v channel are mediated through different mechanisms. Rapidly inactivating (A-type) K_v channels often utilize an N-terminal inactivation domain, a mechanism referred to as "N-type" inactivation. *Shaker-family* N-type inactivation follows a "ball-and-chain" mechanism,[62] where a tethered N-terminal inactivation domain blocks the pore after channel opening, which traps the channel in an open-inactivated state and prevents it from closing.[63] But K_v4 channels (*shal*-family) underlying I_A don't inactivate like this. They accumulate in a closed-inactivated state (I_c) during prolonged depolarization after having only transiently occupied an open-inactivated state (I_o).[64,65] The larger voltage shift of the channel inactivation may be because the binding shifts channel to more stable closed-inactivated state in conformation. Still further studies concerning the structure-function relationship are needed to clarify the binding process.

Though the effect of Natratoxin on voltage-gated A-type K^+ channel has been well proven, whether it can affect other kinds of ion channels is still unclear. Therefore, subsequent studies of Natratoxin will be focused on other targets. Since Natratoxin displays a different fold from other toxins acting on K_v channel, our results were in accordance with previous suggestions that the ability of structurally divergent toxins to recognize a particular ion channel relies on the equivalent spatial distributions of amino acid residues key to the toxin-channel interaction.[17] Compared with β-BuTX, Natratoxin exhibited only weaker inhibitory activity towards the voltage-gated A-type K^+ channel (the IC_{50} values at μ*M* level). To further clarify the possible reasons, additional functional investigations and studies concerning the structure-function relationship are still needed.

CONCLUSIONS

Natratoxin is a novel snake sPLA2 peptide neurotoxin. Our present study revealed it can act as a gating modifier of I_A channel. The 3D structure presented by us will help to illustrate the molecular basis of the interaction between this toxin and I_A channel. Although its overall fold differs from other K^+ channel inhibitors in animal toxins, the identified similar putative functional surface in its C-terminal was suggested to be critical in such a toxin-channel interaction. Our results demonstrated that the spatial distribution of key amino acid residues matters most in the recognition of this toxin towards its channel target rather than its type of fold.

DATA BANK ACCESSION NUMBER

The atomic coordinates of Natratoxin have been deposited in the Protein Data Bank as entry 2OSH.

REFERENCES

1. Wei A, Jegla T, Salkoff L. Eight potassium channel families revealed by the C. elegans genome project. Neuropharmacology 1996;35: 805–829.
2. Tytgat J, Chandy KG, Garcia ML, Gutman GA, Martin-Eauclaire MF, van der Walt JJ, Possani LD. A unified nomenclature for short-

chain peptides isolated from scorpion venoms: alpha-KTx molecular subfamilies. Trends Pharmacol Sci 1999;20:444–447.
3. Yellen G. The moving parts of voltage-gated ion channels. Q Rev Biophys 1998;31:239–295.
4. Armstrong CM. Voltage-gated K channels. Sci STKE 2003;2003: re10.
5. Aggarwal SK, MacKinnon R. Contribution of the S4 segment to gating charge in the Shaker K^+ channel. Neuron 1996;16:1169–1177.
6. Seoh SA, Sigg D, Papazian DM, Bezanilla F. Voltage-sensing residues in the S2 and S4 segments of the Shaker K^+ channel. Neuron 1996;16:1159–1167.
7. Starace DM, Bezanilla F. A proton pore in a potassium channel voltage sensor reveals a focused electric field. Nature 2004;427:548–553.
8. Swartz KJ. Towards a structural view of gating in potassium channels. Nat Rev Neurosci 2004;5:905–916.
9. Tsetlin V. Snake venom alpha-neurotoxins and other "three-finger" proteins. Eur J Biochem 1999;264:281–286.
10. Grishin E. Polypeptide neurotoxins from spider venoms. Eur J Biochem 1999;264:276–280.
11. Possani LD, Becerril B, Delepierre M, Tytgat J. Scorpion toxins specific for Na^+-channels. Eur J Biochem 1999;264:287–300.
12. Garcia ML, Hanner M, Knaus HG, Koch R, Schmalhofer W, Slaughter RS, Kaczorowski GJ. Pharmacology of potassium channels. Adv Pharmacol 1997;39:425–471.
13. Huys I, Olamendi-Portugal T, Garcia-Gomez BI, Vandenberghe I, Van Beeumen J, Dyason K, Clynen E, Zhu S, van der Walt J, Possani LD, Tytgat J. A subfamily of acidic alpha-K(+) toxins. J Biol Chem 2004;279:2781–2789.
14. Menez A. Functional architectures of animal toxins: a clue to drug design? Toxicon 1998;36:1557–1572.
15. Gilquin B, Bourgoin M, Menez R, Le Du MH, Servent D, Zinn-Justin S, Menez A. Motions and structural variability within toxins: implication for their use as scaffolds for protein engineering. Protein Sci 2003;12:266–277.
16. Lewis RJ, Garcia ML. Therapeutic potential of venom peptides. Nat Rev Drug Discov 2003;2:790–802.
17. Mouhat S, Jouirou B, Mosbah A, De Waard M, Sabatier JM. Diversity of folds in animal toxins acting on ion channels. Biochem J 2004;378:717–726.
18. Valentin E, Lambeau G. Increasing molecular diversity of secreted phospholipases A(2) and their receptors and binding proteins. Biochim Biophys Acta 2000;1488:59–70.
19. Rouault M, Rash LD, Escoubas P, Boilard E, Bollinger J, Lomonte B, Maurin T, Guillaume C, Canaan S, Deregnaucourt C, Schrevel J, Doglio A, Gutierrez JM, Lazdunski M, Gelb MH, Lambeau G. Neurotoxicity and other pharmacological activities of the snake venom phospholipase A2 OS2: the N-terminal region is more important than enzymatic activity. Biochemistry 2006;45:5800–5816.
20. Six DA, Dennis EA. The expanding superfamily of phospholipase A(2) enzymes: classification and characterization. Biochim Biophys Acta 2000;1488:1–19.
21. Soragni E, Bolchi A, Balestrini R, Gambaretto C, Percudani R, Bonfante P, Ottonello S. A nutrient-regulated, dual localization phospholipase A(2) in the symbiotic fungus Tuber borchii. Embo J 2001;20:5079–5090.
22. Zadori Z, Szelei J, Lacoste MC, Li Y, Gariepy S, Raymond P, Allaire M, Nabi IR, Tijssen P. A viral phospholipase A2 is required for parvovirus infectivity. Dev Cell 2001;1:291–302.
23. Kini RM. Excitement ahead: structure, function and mechanism of snake venom phospholipase A2 enzymes. Toxicon 2003;42:827–840.
24. Nagiec MJ, Lei B, Parker SK, Vasil ML, Matsumoto M, Ireland RM, Beres SB, Hoe NP, Musser JM. Analysis of a novel prophage-encoded group A Streptococcus extracellular phospholipase A(2). J Biol Chem 2004;279:45909–45918.
25. Chwetzoff S, Tsunasawa S, Sakiyama F, Menez A. Nigexine, a phospholipase A2 from cobra venom with cytotoxic properties not related to esterase activity. Purification, amino acid sequence, and biological properties. J Biol Chem 1989;264:13289–13297.
26. Gutierrez JM, Ownby CL. Skeletal muscle degeneration induced by venom phospholipases A2: insights into the mechanisms of local and systemic myotoxicity. Toxicon 2003;42:915–931.
27. Kini RM. Structure-function relationships and mechanism of anticoagulant phospholipase A2 enzymes from snake venoms. Toxicon 2005;45:1147–1161.
28. Zuliani JP, Fernandes CM, Zamuner SR, Gutierrez JM, Teixeira CF. Inflammatory events induced by Lys-49 and Asp-49 phospholipases A2 isolated from Bothrops asper snake venom: role of catalytic activity. Toxicon 2005;45:335–346.
29. Petersen M, Penner R, Pierau FK, Dreyer F. Beta-bungarotoxin inhibits a non-inactivating potassium current in guinea pig dorsal root ganglion neurones. Neurosci Lett 1986;68:141–145.
30. Dreyer F, Penner R. The actions of presynaptic snake toxins on membrane currents of mouse motor nerve terminals. J Physiol 1987; 386:455–463.
31. Rowan EG, Harvey AL. Potassium channel blocking actions of beta-bungarotoxin and related toxins on mouse and frog motor nerve terminals. Br J Pharmacol 1988;94:839–847.
32. Wu Y, Wang ZF, Shi YL. Beta-agkistrodotoxin inhibits large-conductance calcium-activated potassium channels in rat hippocampal CA1 pyramidal neurons. Brain Res 2002;940:21–26.
33. Leslie AG. Integration of macromolecular diffraction data. Acta Crystallogr D Biol Crystallogr 1999;55:1696–1702.
34. The CCP4 suite: programs for protein crystallography. Acta Crystallogr D Biol Crystallogr 1994;50:760–763.
35. Fremont DH, Anderson DH, Wilson IA, Dennis EA, Xuong NH. Crystal structure of phospholipase A2 from Indian cobra reveals a trimeric association. Proc Natl Acad Sci USA 1993;90:342–346.
36. Jones TA, Zou JY, Cowan SW, Kjeldgaard M. Improved methods for building protein models in electron density maps and the location of errors in these models. Acta Crystallogr A 1991;47(Pt 2): 110–119.
37. Laskowski RA, MacArthur MW, Moss DS, Thornton JM. PROCHECK: a program to check the stereochemical quality of protein structures. J Appl Cryst 1993;26:283–291.
38. Colbert CM, Pan E. Arachidonic acid reciprocally alters the availability of transient and sustained dendritic K(+) channels in hippocampal CA1 pyramidal neurons. J Neurosci 1999;19:8163–8171.
39. Ramakers GM, Storm JF. A postsynaptic transient K(+) current modulated by arachidonic acid regulates synaptic integration and threshold for LTP induction in hippocampal pyramidal cells. Proc Natl Acad Sci USA 2002;99:10144–10149.
40. Scott DL, White SP, Otwinowski Z, Yuan W, Gelb MH, Sigler PB. Interfacial catalysis: the mechanism of phospholipase A2. Science 1990;250:1541–1546.
41. Segelke BW, Nguyen D, Chee R, Xuong NH, Dennis EA. Structures of two novel crystal forms of Naja naja naja phospholipase A2 lacking Ca^{2+} reveal trimeric packing. J Mol Biol 1998;279:223–232.
42. Budde T, Mager R, Pape HC. Different types of potassium outward current in relay neurons acutely isolated from the rat lateral geniculate nucleus. Eur J Neurosci 1992;4:708–722.
43. Kuo CC, Chen FP. Zn(2+) modulation of neuronal transient K(+) current: fast and selective binding to the deactivated channels. Biophys J 1999;77:2552–2562.
44. Pongs O. Voltage-gated potassium channels: from hyperexcitability to excitement. FEBS Lett 1999;452:31–35.
45. Malin SA, Nerbonne JM. Elimination of the fast transient in superior cervical ganglion neurons with expression of KV4.2W362F: molecular dissection of IA. J Neurosci 2000;20:5191–5199.
46. Stewart T, Beyak MJ, Vanner S. Ileitis modulates potassium and sodium currents in guinea pig dorsal root ganglia sensory neurons. J Physiol 2003;552:797–807.

47. Tan ZY, Donnelly DF, LaMotte RH. Effects of a chronic compression of the dorsal root ganglion on voltage-gated Na^+ and K^+ currents in cutaneous afferent neurons. J Neurophysiol 2006;95:1115–1123.
48. Winkelman DL, Beck CL, Ypey DL, O'Leary ME. Inhibition of the A-type K^+ channels of dorsal root ganglion neurons by the long-duration anesthetic butamben. J Pharmacol Exp Ther 2005;314:1177–1186.
49. Fedulova SA, Vasilyev DV, Veselovsky NS. Voltage-operated potassium currents in the somatic membrane of rat dorsal root ganglion neurons: ontogenetic aspects. Neuroscience 1998;85:497–508.
50. Watanabe S, Hoffman DA, Migliore M, Johnston D. Dendritic K^+ channels contribute to spike-timing dependent long-term potentiation in hippocampal pyramidal neurons. Proc Natl Acad Sci USA 2002;99:8366–8371.
51. Chagot B, Escoubas P, Villegas E, Bernard C, Ferrat G, Corzo G, Lazdunski M, Darbon H. Solution structure of Phrixotoxin 1, a specific peptide inhibitor of K_v4 potassium channels from the venom of the theraphosid spider Phrixotrichus auratus. Protein Sci 2004;13:1197–1208.
52. Renisio JG, Lu Z, Blanc E, Jin W, Lewis JH, Bornet O, Darbon H. Solution structure of potassium channel-inhibiting scorpion toxin Lq2. Proteins 1999;34:417–426.
53. Renisio JG, Romi-Lebrun R, Blanc E, Bornet O, Nakajima T, Darbon H. Solution structure of BmKTX, a K^+ blocker toxin from the Chinese scorpion Buthus Martensi. Proteins 2000;38:70–78.
54. Dauplais M, Lecoq A, Song J, Cotton J, Jamin N, Gilquin B, Roumestand C, Vita C, de Medeiros CL, Rowan EG, Harvey AL, Menez A. On the convergent evolution of animal toxins. Conservation of a diad of functional residues in potassium channel-blocking toxins with unrelated structures. J Biol Chem 1997;272:4302–4309.
55. Goldstein SA, Pheasant DJ, Miller C. The charybdotoxin receptor of a Shaker K^+ channel: peptide and channel residues mediating molecular recognition. Neuron 1994;12:1377–1388.
56. Chang CC, Chen TF, Lee CY. Studies of the presynaptic effect of beta-bungarotoxin on neuromuscular transmission. J Pharmacol Exp Ther 1973;184:339–345.
57. Landon DN, Westgaard RH, MacDermot J, Thompson EJ. The morphology of rat soleus neuromuscular junctions treated in vitro with purified beta-bungarotoxin. Brain Res 1980;202:1–20.
58. Su MJ, Chang CC. Presynaptic effects of snake venom toxins which have phospholipase A2 activity (beta-bungarotoxin, taipoxin, crotoxin). Toxicon 1984;22:631–640.
59. Chang CC, Su MJ. Presynaptic toxicity of the histidine-modified, phospholipase A2-inactive, beta-bungarotoxin, crotoxin and notexin. Toxicon 1982;20:895–905.
60. Jeng TW, Hendon RA, Fraenkel-Conrat H. Search for relationships among the hemolytic, phospholipolytic, and neurotoxic activities of snake venoms. Proc Natl Acad Sci USA 1978;75:600–604.
61. Kini RM, Evans HJ. A model to explain the pharmacological effects of snake venom phospholipases A2. Toxicon 1989;27:613–635.
62. Hoshi T, Zagotta WN, Aldrich RW. Biophysical and molecular mechanisms of Shaker potassium channel inactivation. Science 1990;250:533–538.
63. Zagotta WN, Hoshi T, Aldrich RW. Restoration of inactivation in mutants of Shaker potassium channels by a peptide derived from ShB. Science 1990;250:568–571.
64. Jerng HH, Shahidullah M, Covarrubias M. Inactivation gating of K_v4 potassium channels: molecular interactions involving the inner vestibule of the pore. J Gen Physiol 1999;113:641–660.
65. Bahring R, Boland LM, Varghese A, Gebauer M, Pongs O. Kinetic analysis of open- and closed-state inactivation transitions in human $K_v4.2$ A-type potassium channels. J Physiol 2001;535:65–81.